

PRESSURIZED DOWNDRAFT COMBUSTION OF WOODCHIPS

PURNOMO, D. J. AERTS AND K. W. RAGLAND

*Department of Mechanical Engineering
University of Wisconsin
Madison, WI 53706*

A novel biomass fired combustor for a gas turbine powered cogeneration system has been investigated. Experimental results are summarized and a numerical model of the combustor is presented. A 23 cm i.d., downdraft, packed bed combustor has been tested with 2 cm woodchips at pressures to 5 atm with air preheated to 500 K. The woodchips are supported by a bed of refractory gravel. Burning rates over 1000 kg/(hr*m²), dry basis at 13% moisture were obtained. Pressure drop in the bed was about 10%. Particulate emissions averaged 42 ppm. A one dimensional, unsteady, two-phase, reacting, numerical model of the combustor is presented which predicts the fuel burning rate as a function of fuel properties and flow variables. The burning rate is sensitive to combustor pressure, air to fuel ratio, inlet air preheat and fuel properties. Temperature and species profiles were obtained. The reaction zone thickness is typically about 25 mm at 4 atm pressure. Good agreement between the model and experiments was obtained at 1-5 atm and air/fuel of 15-30. Solid and gas temperature, fuel density and species profiles in the combustor were obtained. In contrast to a packed bed a gasifier which has an extended reaction zone. the air flows are high and the reaction zone is thin. At 4 atm pressure the reaction zone thickness is typically about 25 mm.

Introduction

Wood is a renewable, clean burning fuel which contributes significantly to the world energy supply. Wood in, the form of chips allows automated feeding without excessive energy costs for pulverization. Industrial cogeneration of electricity and process heat may be done efficiently using a gas turbine with a heat recovery boiler. Currently pressurized fluidized bed combustors and pressurized gasifiers are under consideration for biomass fired gas turbine combustors.

In this paper we examine the performance of a novel downdraft, packed bed combustor to power a gas turbine. Pioneering work on coal fired downdraft furnaces was done in the late 1940's.^{1,2} Packed bed combustion of coal has been investigated by Essenhigh.³ Downdraft combustion of woodchips has been investigated by Aerts and Ragland.^{4,5} Downdraft gasifiers for biomass have been reviewed by Reed and Das.⁶

A solid fuel fired gas turbine combustor should have a high intensity, exhibit complete carbon utilization, maintain fine flyash particle size, have low pressure drop and good turndown. Downdraft systems typically have better carbon burnup than updraft systems. Maintaining fine ash particles suggests using high excess air to limit peak combustion temperatures. Low pressure drop suggests using

relatively large fuel particle size and minimizing ash deposition.

Experimental Observations

The combustor, fuel feed system and air supply are shown schematically in Fig. 1. Woodchips were fed from a bin through a conveyor to a lockhopper and horizontal screw feeder which provided a continuous supply of fuel. The fuel bed depth typically varied from 20 to 40 cm during a run. Compressed air flowed through a regenerative heater and down through the fuel bed. The refractory and insulation lined combustor had a 23 cm i.d. The tee section was filled with 16 mm diam. alumina or magnesia balls supported at the end of the bed by alumina rods. The combustor pressure was maintained by a downstream water cooled control valve. Further details are given in Ref. 6.

Combustor tests were run with 2 cm yellow-poplar chips. Combustor pressure was varied from 1.1 to 5 atm, inlet air temperature from 298 to 507 K, air to fuel ratio (*a/f*) from 15 to 30, and fuel moisture from 2 to 48%, as received. The burning rate increased as the combustor pressure and inlet air temperature increased and decreased with increasing *a/f* and fuel moisture. Multiple regression analysis on 115 sets of data points yielded the fol-

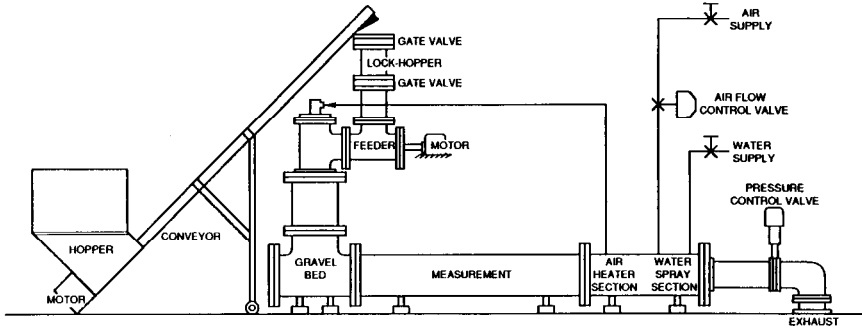


FIG. 1. Test setup for pressurized gravel bed combustor using woodchips.

lowing expression for the burning rate of 2 cm yellow-poplar chips.⁶

$$m_f = 0.42 * p^{0.623} * T^{1.073} * (a/f)^{-0.816} * (100 - M)^{0.600} \quad (1)$$

where m_f is the dry fuel burning rate per unit area, $\text{kg/h}\cdot\text{m}^2$; p is combustor pressure, atm; T is inlet air temperature, K; a/f is air to fuel weight ratio; and M is fuel moisture content, wt.% as received. The correlation coefficient for Eq. 1 is $r^2 = 0.955$, which is excellent. The standard error of the coefficients is 4% for p , 9% for T , 6% for a/f , and 13% for M .

Carbon monoxide emissions were above 2000 ppm until the bed outlet temperature rose above 1050 K; then the CO dropped to several hundred ppm, typically. Thus for an adiabatic bed the a/f should be less than 25 for low CO emissions. The NO emissions ranged from 10 to 285 ppm and averaged 75 ppm. There was essentially no sulfur in the fuel. Hydrocarbons were not measured. Exhaust particulates averaged 42 ppm (by wt.) of which 30% was carbon, on the average. Bed pressure drop varied from 3 to 17% with the alumina bed and from 5 to 10% with the magnesia bed. Ash deposition to the bed occurred with the alumina but was minimal with the magnesia bed. The goal is to hold the pressure drop under 10% and operate hundreds of hours without a bed change.

Downdraft Combustor Model

Consider a bed of fuel particles supported by a bed of refractory gravel. Air flows downward through the fuel bed which undergoes drying, pyrolysis and char burn. In the drying and pyrolysis zones the fuel volume and velocity remain constant as the density decreases. In the char zone the fuel density remains constant and the diameter shrinks causing the fuel velocity to gradually decrease to zero at

the gravel interface. Conservation of mass and energy for the solid and gaseous phases are formulated in one-dimensional unsteady form.⁷

Conservation of mass for drying, pyrolysis and char burn are given below and the source terms are given in Table I,

$$\frac{\partial \rho_m}{\partial t} + V_s \frac{\partial \rho_m}{\partial z} = -r_m \quad (2)$$

$$\frac{\partial \rho_p}{\partial t} + V_s \frac{\partial \rho_p}{\partial z} = -r_p \quad (3)$$

TABLE I
Source or reaction rate equations

Rate Equations	Reference
$r_m = A_m(\rho_s - \rho_d) \exp(-E_m/RT_s)(1 - \delta)$	(8)
$r_p = A_p(\rho_s - \rho_c) \exp(-E_p/RT_s)(1 - \delta)$	(9)
$r_c = A_c \phi p_{O_2}^n (M_g/M_s) 2 k_r \tilde{h}_D / ((M_g/M_s) k_r + 2\tilde{h}_D)$	(10)
$r_{HC} = A_{HC} T_e p^{0.3} [HC]^{0.5} [O_2] \exp(-E_{HC}/RT_e)$	(10)
$r_{CO} = A_{CO} [CO][O_2]^{0.25} [H_2O]^{0.5} \exp(-E_{CO}/RT_e)$	(10)
where, $k_r = A_c \exp(-E_c/RT_s)$	
$\tilde{h}_D = 1.57 G_g Sc^{-2/3} Re^{-0.41}$	
$(1 - \delta)^{0.2} / M_g p$	(11)
$T_e = \alpha T_g + (1 - \alpha) T_s$, if $T_g \leq T_s$;	
$T_e = T_g$ if $T_g > T_s$,	
$Re = 6G_g / A_c \phi \mu$; $A_c = 6(1 - \delta) / d_s$;	
$d_s = (A_s / \pi)^{1/2}$	

$$(1 - \delta) \rho_c \frac{\partial V_s}{\partial z} = -r_c \quad (4)$$

The overall mass balance in the gas phase within the fuel and gravel bed is,

$$\delta \frac{\partial \rho_g}{\partial t} + \frac{\partial G_g}{\partial z} = r_m + r_p + r_c \quad (5)$$

The gas phase consists of oxygen, hydrocarbons, carbon monoxide, carbon dioxide, and water vapor from drying, pyrolysis and combustion which vary with time and position, and nitrogen for which the mass flux remains constant. The assumed pyrolysis products are shown in Table II. The hydrocarbons, including tars react to form hydrogen and CO according to the global reaction rate given in Table I and rate parameters given in Table III. Hydrogen from pyrolysis is assumed to react instantly to form

water vapor. The CO then reacts to form CO₂. The species mass balances are given by:
Oxygen:

$$\delta \frac{\partial \rho_{O_2}}{\partial t} + \frac{\partial (G_g x_{O_2})}{\partial z} = -0.5 r_p x_{H_2} (M_{O_2}/M_{H_2}) - (0.5a + 0.25b - 0.5c) r_{HC} (M_{O_2}/M_{HC}) - 0.5 r_c (M_{O_2}/M_c) \quad (6)$$

Hydrocarbons:

$$\delta \frac{\partial \rho_{HC}}{\partial t} + \frac{\partial (G_g x_{O_2})}{\partial z} = r_p x_{HC} - r_{HC} M_{HC} \quad (7)$$

Carbon monoxide:

$$\delta \frac{\partial \rho_{CO}}{\partial t} + \frac{\partial (G_g x_{CO})}{\partial z} = r_p x_{CO} - r_{CO} M_{CO} + r_{HC} M_{CO} + r_c (M_{CO}/M_c) \quad (8)$$

Carbon dioxide:

$$\delta \frac{\partial \rho_{CO_2}}{\partial t} + \frac{\partial (G_g x_{CO_2})}{\partial z} = r_p x_{CO_2} + r_{CO} M_{CO_2}/M_{CO} \quad (9)$$

Water vapor:

$$\delta \frac{\partial \rho_{H_2O}}{\partial t} + \frac{\partial (G_g x_{H_2O})}{\partial z} = r_p x_{H_2O} + r_p x_{H_2} (M_{H_2O}/M_{H_2}) + 0.5b r_{HC} M_{H_2O} + r_m \quad (10)$$

TABLE II
Equivalent composition of dry wood (13,7)

Component	Mass Fraction, X _i
char	0.200
hydrocarbons*	0.247
hydrogen	0.005
carbon monoxide	0.115
carbon dioxide	0.250
water vapor	0.183

*C_aH_bO_c; a = 1, b = 0.335, c = 0.00461.

TABLE III
Reaction rate parameter values

Parameter	Value	Reference
A _m	2 × 10 ¹⁰ hr ⁻¹	(7)
E _m	2.1 × 10 ⁴ cal/mol	(7)
A _p	2.52 10 ¹¹ hr ⁻¹	(8)
E _p	3.0 × 10 ⁴ cal/mol	(8)
A _{CO}	6.4 × 10 ⁷ (see reaction rate)	(9)
E _{CO}	4.0 × 10 ⁴ cal/mol	(9)
A _{HC}	1.0 × 10 ⁸ (see reaction rate)	(9)
E _{HC}	1.917 × 10 ⁷ cal/mol	(9)
A _c	1.71 × 10 ⁷ kg/m ² hr	(17)
E _c	23.8 × 10 ⁴ cal/mol	(17)
H _c	9.975 MJ/kg	
H _{CO}	9.975 MJ/kg	
H _{H₂}	120 MJ/kg	
H _{HC}	19.67 MJ/kg	
n	1.25	by adjustment

Conservation of energy in the solid phase includes heat conduction due to an effective conductivity which includes radiation, downward convection of the solid, heat transfer between the gas and solid, and chemical reaction at the solid surface. The char reacts to form carbon monoxide at a rate which includes kinetic and turbulent diffusion factors, as indicated in Table I. As the char particles shrink the transport properties are updated. Conservation of energy for the solid phase is,

$$(1 - \delta) \frac{\partial(\rho_s u_s)}{\partial t} + \frac{\partial(G_s h_s)}{\partial z} = \frac{\partial}{\partial z} \left(k_e \frac{\partial T_s}{\partial z} \right) + \tilde{h} A_v \phi (T_g - T_s) - r_m h_m - r_p h_p + r_c H_c \quad (11)$$

where heat transfer parameters k_e and h are defined in Table IV. Conservation of energy for the gas phase has a similar form,

$$\delta \frac{\partial(\rho_g u_g)}{\partial t} + \frac{\partial(G_g h_g)}{\partial z} = \frac{\partial}{\partial z} \left(k_g \frac{\partial T_g}{\partial z} \right) + \tilde{h} A_v \phi (T_s - T_g) + r_m h_m + r_p h_p + r_{CO} H_{CO} + r_{HC} H_{HC} \quad (12)$$

Two boundary conditions are needed for both the solid and gaseous energy equations. At the top of the fuel bed the fuel and gas temperature are set equal to the inlet air temperature, because the fuel bed is relatively thick and it will be seen that the reaction zone is thin in this application. At the bottom of the gravel bed the temperature is not known, but the temperature gradient is set by heat transfer and chemical reaction,

$$k_e \frac{\partial T_s}{\partial z} = \tilde{h} A_v \phi (T_g - T_s) \quad (13)$$

$$k_g \frac{\partial T_g}{\partial z} = \tilde{h} A_v \phi (T_s - T_g) + r_{CO} H_{CO} + r_{HC} H_{HC} \quad (14)$$

The right hand side of Eqs. 13 and 14 are usually zero, but are important during startup and are in-

cluded in the finite difference equations to provide less restrictive implicit boundary conditions.

The governing equations contain twelve unknowns ($\mathbf{r}_s, \mathbf{r}_{pp}, \mathbf{r}_p, V_s, G_g, X_{O_2}, X_{H_2O}, X_{HC}, X_{CO}, X_{CO_2}, T_s$ and T_g). Initial conditions are given for each variable based on unreacting conditions, and an initial char temperature is specified for startup. The property values used for yellow-poplar woodchips and alumina bed material are given in Table V.

A fully implicit finite difference method was used to solve the equations. The reaction source terms are highly nonlinear and tightly couple the energy equations with the mass balance equations. Linearization and underrelaxation were used to maintain stability of the solution. A central differencing scheme was used for the second order terms, and backward differencing was used for the first order terms. Scalar variables were defined at the center of the control volume, and non-scalar variables (velocity and mass flux) were defined at the boundaries of the control volume. Upwind differencing with a staggered grid was used for the convective terms. The difference equations for the gas and solid energy equations were solved using the Thomas algorithm. The forward step started from the bottom of the bed and the back substitution began from the top. The computation started at the top of the fuel bed, except for fuel velocity which started from the gravel interface where V_s is zero. The iteration procedure was as follows: 1) assume an initial solid temperature profile allowing for a reacting char layer with fuel on top; 2) calculate all temperature dependent properties; 3) solve the mass balance equations sequentially; 4) solve the energy equations iteratively; 5) with the new temperature profile return to step 2, and repeat until the gas temperature (found to be the most sensitive parameter) convergence error is sufficiently small (5×10^{-4}). The grid size was 1 mm in the fuel bed and 2.5 mm in the gravel bed. The time step was 10^{-4} hr. A transient formulation was needed to obtain a steady state solution. Reducing the grid size and time step by a factor of 2 changed the burning rate by less than 0.5%. The fuel thickness was 15 cm and the gravel thickness 25 cm. The time to steady state was typically 800 s so there were about 3000 time steps. A model run took about 4 min on a CRAY X-MP/48 computer. To insure that the converged solution was valid the overall C, H, O mass balances and overall energy balance were checked at steady state. Agreement was obtained to within a fraction of a percent.

TABLE IV
Heat transfer relationships

Relationship	Reference
$k_e = k_s(\gamma + (1 - \delta)\beta)/(1 + k_s/d_s h_{rs}) + d_s h_{rv}/k_s$	(12)
$\tilde{h}_{rs} = 4\sigma T_s^3 (2 - \epsilon)/\epsilon$	(12)
$\tilde{h}_{rv} = 4\sigma T_s^3/(1 + \delta(1 - \epsilon)/2\epsilon(1 - \delta))$	(12)
$\tilde{h} = 1.57c_{pg} C_g Pr^{-2/3} Re^{-0.41}(1 - \delta)^{0.2}$	(11)

Discussion of Modeling Results

In order to improve agreement between the model and the experiments several adjustments had to be made. This is justified due to the different

TABLE V
Physical, thermodynamic and transport property values

Parameter	Value	Reference
$\delta(\text{fuel})$	0.45	
$\delta(\text{gravel})$	0.45	
$\phi(\text{fuel})$	0.86	
$\phi(\text{gravel})$	1.0	
β	1.0	
ϵ	0.8	
$A_s(\text{fuel})$	12.6 cm ² for 1.91 cm nominal chip	(7)
$d_s(\text{gravel})$	1.6 cm	
$\rho(\text{moisture})$	1000 kg/m ³	
$\rho(\text{dry fuel, initial})$	470 kg/m ³	
$\rho(\text{char})$	94 kg/m ³	
$\rho(\text{gravel})$	3970 kg/m ³	(7)
$c(\text{moisture})$	4200 J/kg · K	
$c(\text{fuel, dry})$	1380 J/kg · K	(14)
$c(\text{char})$	650 J/kg · K	(14)
$c(\text{gravel})$	765 J/kg · K	(15)
$k(\text{fuel})$	0.144(1.39 + 2.8X _m + 0.165)($\rho_f/1000$) W/m · K	(16)
$k(\text{char})$	0.041 T _s /298 W/m · K	(13)
$k(\text{gravel})$	8.0 W/m · K	(15)
$k(\text{gas})$	4.8 × 10 ⁻⁴ T _g ^{0.717} W/m · K	(11)
$\mu(\text{gas})$	1.98 × 10 ⁻⁵ (T _g /300) ^{2/3} N · s/m ²	
$D(\text{gas})$	1.78 × 10 ⁻⁵ (T _g /300) ^{1.75} m ² /s	
$Pr(\text{gas})$	0.708	

conditions of the model compared to the original experimental correlations reported in the literature, particularly with respect to turbulence and chemical reaction. The heat transfer coefficient was divided by 4 and the mass transfer coefficient by 2. The hydrocarbon and carbon monoxide activation energies were divided by 1.33. The parameter α was introduced (in Table I) to obtain an effective temperature for the gas phase reaction rates because the gas is flowing through a packed bed of very irregular fuel particles. The effective temperature, which was higher than the gas temperature and lower than the solid temperature, was a way to account for backmixing due to the chips. Backmixing increases the residence time, and decreasing the reaction time due to the higher temperature has the same effect as increasing the residence time. A value of $\alpha = 0.4$ gave good results. The char reaction rate was relatively insensitive to pressure because h_D varies inversely with pressure, and it was found that a value of $n = 1.25$ rather than the literature value of 1.0 gave better results when comparing the model fuel burning rate with the experiments. Also, the drying rate constant was adjusted.

Startup of the model was done at reduced air flow and temperatures, and then the air flow was automatically adjusted to meet a specified exhaust ox-

xygen level. Steady state was typically reached in 10-15 min of simulation time. Only the steady state results are presented here. The temperature and density profiles for representative conditions at 4 atm pressure are shown in Fig. 2. The fuel dries as the gas and solid temperatures equilibrate. In this case the fuel is dried completely to 370 kg/m³ before entering the reaction zone. At 3.5 cm above the gravel pyrolysis begins, the fuel density drops rapidly and the solid temperature rises rapidly. Hence the reaction zone is very thin compared to the reaction zone in a pressurized gasifier, which agrees with our experimental observations in a small 10 cm i.d. quartz tube combustor at atmospheric pressure. In Fig. 2 the pyrolysis zone is less than 1 mm thick and the char reaction zone is 30 mm thick.

Hydrocarbons and carbon monoxide emitted during pyrolysis are swept downstream and react in the char zone (see Fig. 3). By exercising the model it was observed that the volatiles must burnout in the char zone, or otherwise the reaction zone becomes too thin and blowout occurs. The CO which forms from the char reaction reacts rapidly. In the reaction zone the solid temperature exceeds the gas temperature by up to 270 K due to the char surface reaction and subsequent heat conduction. The temperatures equilibrate rapidly in the gravel bed.

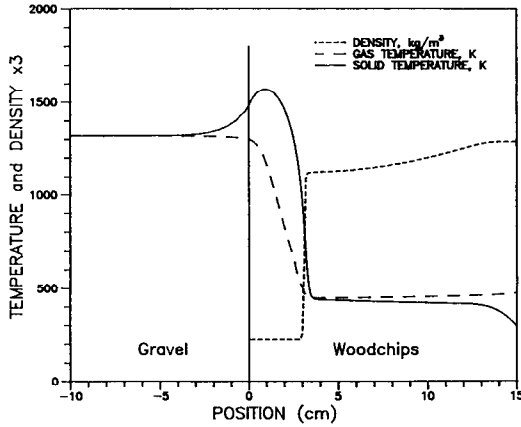


FIG. 2. Model temperature and density profiles in the fuel bed and gravel; 2 cm yellow-poplar chips with 13% moisture, 4 atm, 473 K inlet air, and $af = 20$.

A map of fuel burning rate per unit cross-sectional area of the combustor versus inlet air flux and combustor pressure is shown in Fig. 4. The combustor is operated lean to reduce peak temperature. In practice this means af greater than 15 (adiabatic flame temperature less than 1380 K at 13% wood moisture). Above af ratio of 30 the burning rate is too slow (adiabatic flame temperature is 975 K). For yellow-poplar stoichiometric af is 6.3, and thus the operating regime is 140% to 280% excess air. For this operating regime, as seen in Fig. 4, both experimentally and with the model, the burning rate decreases with increasing air flow. As the air flow increases the reaction zone becomes thinner because convection downstream

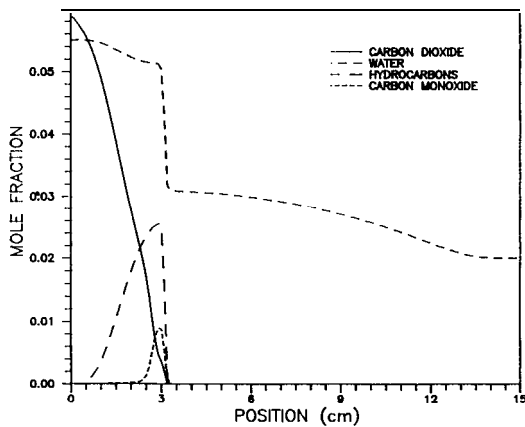


FIG. 3. Model species profiles in the fuel bed; 2 cm yellow-poplar chips with 13% moisture, 4 atm, 473 K inlet air, and $af = 20$.

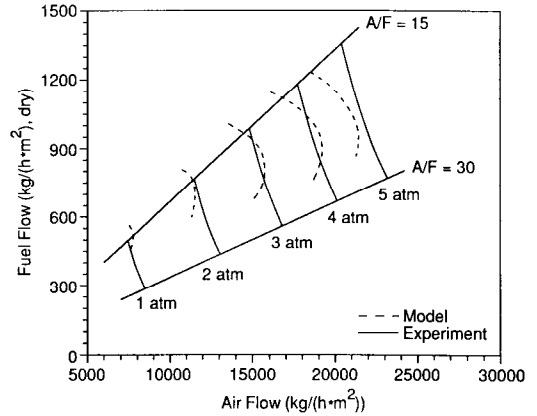


FIG. 4. Effect of air flow rate and pressure on burning rate; 2 cm yellow poplar chips with 13% moisture and 473 K inlet air.

exceeds heat conduction and radiation heat transfer upstream as the temperature drops and the reaction rates slow down. Increasing the combustor pressure results in a higher burning rate since more oxygen is available, and to maintain the same amount of excess air and thus control the temperature, the air flow must be increased. The volatile reaction rates increase with pressure (see Table I). As indicated above increasing the char pressure sensitivity power n from 1 to 1.25 in the char reactivity gave improved agreement between the model and experiment.

The model was operated by automatically increasing the air in increments to hold the exhaust oxygen concentration at a preset value. If the exhaust oxygen was set too high (say 15%) the flame would blowout. At slightly lower exhaust oxygen values the model seeks a solution by decreasing both the air flow and the fuel flow rates. For a given air flow the model gives two possible fuel flows (see Fig. 4). The experimental curves on the other hand maintain a negative slope over the operating range. At any lean operating point, gradually increasing the air flow decreases the burning rate. Increasing the air flow beyond a certain value causes blowout. At each pressure level there is a relatively narrow operating range of air flows. The burning rate is very sensitive to pressure and air flow rate. The reaction zone thickness decreases with increasing air flow. The reaction zone thickness at maximum air flow is 26 mm at 4 atm pressure according to the model and this occurs at an af of 24. Increasing the pressure decreases the minimum sustainable reaction zone thickness. Experimentally blowout occurs near af of 30.

As noted above, the burning rate is also sensitive to inlet air temperature and fuel moisture content,

The model correctly predicts that the burning rate increases with increasing inlet air temperature and decreases with fuel moisture, however the model overpredicts the experimental trends. Further modeling and experiments are needed to examine this point.

Industrial gas turbines typically run at turbine inlet temperatures of 1200-1400 K. Lower temperatures reduce engine efficiency while higher temperatures degrade the turbine blades. Thus for woodchips the combustor should be run at an *af* of 15-20. This allows for a reasonable match between turbine and combustor requirements without compressor air bypassing the combustion zone. Further study of ash deposition, combustor pressure drop and control of the combustor when coupled to a compressor-turbine are being conducted.

Conclusions

A novel downdraft combustor has been tested with woodchips at pressures to 5 atm. Combustion is intense and the reaction zone is thin compared to a gasifier. A one dimensional, unsteady, two-phase, reacting, numerical model of the combustor has been developed which predicts the measured fuel burning rate as a function of fuel properties and flow variables. These results indicate that testing and modeling of a downdraft combustor-gas turbine system are justified.

Nomenclature

A_i	pre-exponential factor, hr^{-1}
A_s	surface area, cm^2
A_c	surface area per unit volume, cm^{-1}
c	specific heat, $\text{J}/(\text{kg} \cdot \text{K})$
d_s	equivalent particle diameter, cm
D	diffusivity of oxygen, m^2/s
E	activation energy, cal/mol
G	mass flux, $\text{kg}/\text{m}^2 \cdot \text{hr}$
\bar{h}	heat transfer coefficient, $\text{W}/(\text{m}^2 \cdot \text{K})$
\bar{h}_D	mass transfer coefficient, $\text{kg}/(\text{s} \cdot \text{m}^2)$
h_s	enthalpy of solid, kJ/kg
h_i	enthalpy of gas i , kJ/kg
h_{rs}	surface to surface radiation heat transfer coefficient
h_{rv}	void to void radiation heat transfer coefficient
H_i	heat of reaction, MJ/kg
k_e	effective solid conductivity, $\text{W}/(\text{m} \cdot \text{K})$
k_s	solid conductivity, $\text{W}/(\text{m} \cdot \text{K})$
k_g	effective gas conductivity, $\text{W}/(\text{m} \cdot \text{K})$
k_r	rate constant
M	molecular weight, $\text{kg}/\text{kg mol}$
n	empirical exponent
p	pressure, atm
Pr	Prandtl Number

R	universal gas constant, $\text{kJ}/(\text{kg mol} \cdot \text{K})$
Re	Reynolds Number
r_{HC}	hydrocarbon reaction rate per unit combustor volume, $\text{kg}/(\text{m}^3 \cdot \text{s})$
r_{CO}	CO reaction rate per unit combustor volume, $\text{kg}/(\text{m}^3 \cdot \text{s})$
r_C	char reaction rate per unit combustor volume, $\text{kg}/(\text{m}^3 \cdot \text{s})$
r_p	pyrolysis rate per unit combustor volume, $\text{kg}/(\text{m}^3 \cdot \text{s})$
r_m	moisture release rate per unit combustor volume, $\text{kg}/(\text{m}^3 \cdot \text{s})$
Sc	Schmidt Number
T	absolute temperature, K
t	time, s
u	internal energy, kJ/kg
V_s	solid velocity, m/s
x_i	mass fraction of constituent i ($i = \text{CO}, \text{CO}_2, \dots$)
X_i	mass fraction of pyrolysis products (see Table II)
z	vertical distance, m
α	weighting factor
β	geometry factor
γ	contact area/total area
δ	void fraction
ϵ	surface emissivity
ϕ	shape factor
ρ_v	volatile matter density in wood, kg/m^3
ρ_m	moisture density in wood, kg/m^3
ρ_c	char density, kg/m^3
ρ_d	dry fuel density, kg/m^3
ρ_s	solid density, kg/m^3
σ	Steffan-Boltzman constant, $\text{W}/(\text{m}^2 \cdot \text{K}^4)$
μ	viscosity, $\text{N} \cdot \text{s}/\text{m}^2$

Acknowledgments

The authors thank Carl Palmer for obtaining the experimental correlation of the data. The woodchips were provided by Andrew Baker at the U.S. Forest Products Laboratory. The continued FPL assistance and initial funding of the project are gratefully acknowledged. The work was supported by the U.S. Department of Energy under grant DE-FG02-85CE40735. Chris Sperry, Eric Earhart, Eric Wiley and John Wold assisted with the experiments.

REFERENCES

1. LANDRY, B. A. AND SHERMAN, R. A.: ASME Transactions, 72, 9 (1950).
2. See Chemistry of Coal Utilization, 2nd Supplementary Volume, (M. A. Elliott, Ed.), p. 1339, Wiley, 1981.
3. GOLDMAN, J., XIEW, D., OKO, A., MILNE, R.

- AND ESSENHIGH, R. H.: Twentieth Symposium (International) on Combustion, p. 1365, The Combustion Institute, 1985.
4. RAGLAND, K. W., AERTS, D. J. AND BAKER, A. J.: Research in Thermochemical Biomass Conversion, (A. L. Bridgewater and J. L. Kuester, Ed.), p. 744, Elsevier Press, 1988.
 5. RAGLAND, K. W. AND AERTS, D. J.: Development of a Gravel Bed Combustor for Solid Fueled Gas Turbine, U.S. DOE report DE/CE/40735-1, 1989.
 6. REED, T. B. AND DAS, A.: Handbook of Biomass Downdraft Gasifier Engine Systems, U.S. Dept. of Energy, SERI/SP-271-3022, DE88001135, 1988.
 7. PURNOMO: Model for a Downdraft Solid Fuel Combustor, Ph.D. thesis, The University of Wisconsin-Madison, 1988.
 8. CHAN, W. R. et al: Fuel, 64, 1505 (1985).
 9. ROBERTS, A. F.: Comb. Flame, 14, 261 (1970).
 10. SMOOT, L. D. AND SMITH, P. J.: Coal Combustion and Gasification, Plenum Press, New York, 1985.
 11. GAMSON, B. W.: Chem. Eng. Prog., 47, 19 (1951).
 12. YAGI, S. AND KUNII, D.: AIChE Journal, 3, 373 (1957).
 13. ADAMS, T. N.: Comb. Flame, 39, 225 (1980).
 14. KUNG, H. C. AND ASHOK, S. K.: Comb. Flame, 20, 91 (1973).
 15. VAN VLACK, L. H.: Elements of Materials Science and Engineering, 3rd ed., p. 470, Addison Wesley, 1975.
 16. MACLEAN, J. D.: Heating, Piping and Air Conditioning, 13, 380 (1941).
 17. BHAGAT, P. M., Comb. Flame, 37, 275 (1980).